This is the peer-reviewed, final accepted version for American Mineralogist, published by the Mineralogical Society of America.
The published version is subject to change. Cite as Authors (Year) Title. American Mineralogist, in press.
DOI: https://doi.org/10.2138/am-2021-7928. http://www.minsocam.org/

REVISION 1

Elastic geobarometry: how to work with residual inclusion strains and pressures

Mattia Gilio[1], Ross J. Angel[2] and Matteo Alvaro[1]

[1]Department of Earth and Environmental Sciences, via Ferrata, 4, University of Pavia, Pavia, Italy
[2]IGG-CNR, Via G. Gradenigo, 6, Padova, Italy

Abstract

A continuously increasing number of research groups are adopting elastic geobarometry for retrieving pressures and temperatures of entrapment of inclusions into a host from both natural and experimental samples. However, a few misconceptions of some of the general concepts underlying elastic geobarometry are still widespread. One is the difference between various approaches to retrieve the residual pressures and residual strains from Raman measurements of inclusions. In this paper, the estimation of uncertainties and the validity of some general assumptions behind these methods are discussed in detail and we provide general guidelines on how to deal with inclusion strain, measurements, inclusion pressure and their uncertainties.

Introduction

Elastic geobarometry is a useful tool to estimate the pressure and temperature (PT) of equilibration of a mineral assemblage starting from the residual pressure of inclusions trapped in a host. Consider a soft inclusion in a stiffer host (e.g., quartz in garnet) entrapped at a certain PT_{trap} condition and exhumed to the surface (PT_{end}). At PT_{end} conditions, both host and inclusion have a larger volume than at entrapment, due to pressure being released upon exhumation ($\Delta V>0$). However, the volume increase of the softer quartz should be greater than that of the stiffer host ($\Delta V_{qz}>\Delta V_{grt}$). The host garnet compresses the quartz inclusion into a smaller volume than a free quartz crystal, straining and pressurizing the inclusion. Knowing the inclusion pressure (P_{inc} = mean normal stress) at T_{end} (normally room T) and the elastic properties of host and inclusion allows one to back-calculate a line in PT space of possible entrapment conditions: the isomeke (e.g. Angel et al., 2017b; Angel et al., 2014; Rosenfeld and Chase, 1961).

Several authors have worked on developing an accurate Raman calibration for quartz at high pressure and temperature conditions (Morana et al., 2020; Schmidt and Ziemann, 2000). These calibrations, originally aimed at developing an alternative pressure sensor to ruby fluorescence for experiments at room temperature, have found extensive use in metamorphic petrology to determine the residual pressures of mineral inclusions trapped in mineral hosts (Enami et al., 2007; Kohn, 2014; Thomas and Spear, 2018; Zhong et al., 2019). However, this application is subject to several limitations. One of the major assumptions of this method is the quasi-linear dependency of inclusion pressure and the change in Raman peak position (hereafter $\Delta\omega = \omega_i - \omega_0$, where ω_i is the Raman shift of a certain mode of the inclusion and ω_0 is the Raman shift of the same mode in an unstrained, free reference crystal). However, this is essentially incorrect, as the wavenumber shift of a phonon mode m in a crystal ($\Delta\omega^m$) depends on the imposed strain rather than pressure. This relation is described by a second-rank symmetric tensor: the phonon-mode Grüneisen tensor $\boldsymbol{\gamma^m}$ (Ziman, 1960) which, for uniaxial crystals (e.g., quartz and zircon), can be expressed as $\frac{-\Delta\omega^m}{\omega_0^m} = 2 * \gamma_1^m * \varepsilon_1 + \gamma_3^m * \varepsilon_3$, where γ_1^m and γ_3^m are the components of $\boldsymbol{\gamma^m}$ in Voigt notation (Angel et al., 2019). Using the concept of phonon-mode Grüneisen tensor, Murri et al. (2018) developed a method to estimate the strain-state of an inclusion using measurements of multiple Raman modes. The inclusion strain is then converted to stress with a stiffness tensor (e.g., Wang et al. (2015) for quartz) to obtain the inclusion stress state from which we calculate the mean normal stress (which we equate to pressure). Despite this new technique, several authors still adopt the direct Raman-shift to inclusion pressure conversion from hydrostatic hydrothermal-diamond anvil cell calibrations regardless of the symmetry of the inclusion and the host (e.g., Cisneros et al., 2020; Dunkel et al., 2020; Wolfe and Spear, 2020; Zhong et al., 2019). This would not be a major problem for a cubic inclusion in a cubic host in which the isotropic strain imposed by the host creates an isotropic (hydrostatic) stress in the inclusion. However, an elastically anisotropic inclusion in a (near-) isotropic host (e.g., quartz in garnet) develops non-hydrostatic deviatoric stresses when subjected to an isotropic strain. In some cases, discrepancies between the two methods can be small, while in some other cases errors may be large enough to lead to incorrect interpretations. Here, we compare the results of these two methods for determining the inclusion pressures of quartz inclusions in garnet from both natural (Syros Island, Greece, Cisneros et al., 2020; eastern Papua New Guinea, Gonzalez et al., 2019) and experimental (Bonazzi et al., 2019) samples and we discuss whether the hydrostatic approximation is a viable alternative to the anisotropic model for retrieving the inclusion pressure. Furthermore, we show how inclusion strain analysis can provide new information on the strain and stress state of the rocks at entrapment conditions.

This is the peer-reviewed, final accepted version for American Mineralogist, published by the Mineralogical Society of America.
The published version is subject to change. Cite as Authors (Year) Title. American Mineralogist, in press.
DOI: https://doi.org/10.2138/am-2021-7928. http://www.minsocam.org/

Inclusion strain vs. inclusion pressure

The comparison between the two approaches (i.e., Grüneisen tensor vs hydrostatic calibration) can be easily demonstrated with a diagram that represents the principal independent strain components for a quartz inclusion trapped in garnet together with their inclusion pressure. **Figure 1** is a $\varepsilon_1+\varepsilon_2$ vs ε_3 graph showing the strains of quartz inclusions in garnet from Syros (Cisneros et al., 2020), Papua New Guinea (Gonzalez et al., 2019) and from piston-cylinder press experiments (Bonazzi et al., 2019). These inclusion strains were calculated from their $\Delta\omega$ for ω_{128}, ω_{206}, ω_{264} (when available) and ω_{464} using the Grüneisen tensor of Murri et al. (2018) and the software stRAinMAN (Angel et al., 2019). **Figure 1** is also contoured in values of P_{inc}, calculated in two ways. The black lines are P_{inc} calculated by converting the strains into stresses using the adiabatic elastic tensor at 1 bar by Wang et al. (2015) and considering the inclusion pressure as the mean normal stress $\left(P_{inc} = \frac{\sigma_1+\sigma_2+\sigma_3}{3}\right)$. Using a different formulation of the elastic tensor of quartz at 1 bar (such as the one by Mazzucchelli et al., 2020) has a negligible effect on the position of the lines of equal P_{inc}. This approach ignores the stiffening of the elastic moduli of quartz with pressure (see the detailed discussion in the supplementary materials). Adopting the elastic tensor measured at 1.4 GPa (Wang et al. (2015), which might be more consistent with the pressures exhibited by these inclusions, produces changes in the absolute P_{inc} values and reduces the spacing between the black "isobars", while maintaining their slope unchanged. The red lines in Figure 1 represent the P_{inc}^{464}, as would be obtained by measuring only the shift of the 464 cm^{-1} Raman band of a quartz inclusion and converting it to pressure via the hydrostatic calibration $P_{inc}^{464} = \left(0.00029 * \Delta\omega_{464}{}^2 + 0.118 * \Delta\omega_{464}\right) GPa$ by Morana et al. (2020), which is equivalent to the calibration by Schmidt and Ziemann (2000) for P < 2.1 GPa. The two sets of lines (equal P_{inc} and P_{inc}^{464}) are non-parallel and cross at an angle of about 13.3°. This implies that at any given strain condition P_{inc} is different from P_{inc}^{464} with the sole exception of the origin (at zero strains) and near the line of hydrostatic conditions. Using the hydrostatic calibration of different Raman modes (e.g., ω_{206}; Morana et al., 2020; Schmidt and Ziemann, 2000) leads to analogous results to the ω_{464}.

Uncertainties in measurements and data processing

The measured Raman shift of a strained inclusion has an intrinsic uncertainty arising from the instrumental reproducibility and the fitting procedure. This uncertainty is generally ~0.35 cm^{-1} for the best-performing instruments at moderate wavenumber values (100-1000 cm^{-1}) but it can be larger for low performance instruments and for low intensity modes (e.g., ω_{264}). After converting the shifts into strain, the 2σ uncertainty is then represented as in **Figure 1** using covariance ellipses calculated from the covariance matrix. These extremely elongated ellipses highlight the large correlations existing between the two strains arising from the similar strain dependence of the independent modes (see Angel, 2000 for more details on covariance ellipses and parameter correlation). The confidence ellipses for quartz are subparallel to the lines of equal P_{inc}. Therefore the precision of the absolute values of the independent strain components (ε_1, ε_2 and ε_3) is low, while the precision on the P_{inc} is high (its uncertainty is generally < 0.1 GPa; see Mazzucchelli et al., 2020 for the uncertainty conversion procedure). As an example, in **Figure 1** the red and orange circles represent the strains determined on quartz inclusions in almandine synthesized using piston-cylinder press experiments (Bonazzi et al., 2019) under controlled PT conditions of 775 °C – 3.0 GPa and 800 °C – 2.5 GPa, respectively. Despite the large variations in strains along the isobars, all inclusions have a similar P_{inc} (weighted average at 1.15±0.02 GPa for alm 1 and 0.95±0.02 GPa for alm 2) and plot subparallel to the lines of equal P_{inc}. We can see this type of scattering in natural samples as well: the inclusions strains of quartz inclusions from Syros (Cisneros et al., 2020) and Papua New Guinea (Gonzalez et al., 2019) in **Figure 1** line up within their uncertainty ellipses and are subparallel to the lines of equal P_{inc}. This is not the case for the lines of equal P_{inc}^{464} (red lines in **Figure 1**), which means that the hydrostatic method can lead to significantly different pressures for a set of inclusions entrapped at the same PT condition (e.g., piston-cylinder press experiment). As an example, the P_{inc} calculated for quartz inclusions from alm 1 (Bonazzi et al., 2019) is 1.15±0.02 GPa, while the P_{inc}^{464} ranges from ~0.6 to ~1.3 GPa (**Figure 1**).

In **Figure 2a**, we can see that the difference between P_{inc} and P_{inc}^{464} increases with volume strain ($\varepsilon_V = \varepsilon_1 + \varepsilon_2 + \varepsilon_3$) both along the hydrostatic stress and the isotropic strain lines (yellow and green dashed lines in the figure). Also, this increase is exponential, with relatively small differences in P_{inc} (~0.02) for small strains. This is because the P_{inc}^{464} of quartz was calibrated under hydrostatic stress condition within a diamond-anvil. As such, the direct correlation ω_{464}-to-P_{inc} gives similar results to the inclusion mean normal stress under hydrostatic conditions. However, the strain state of quartz inclusions in garnet suggests that such inclusions are under non-hydrostatic stress conditions (**Figure 1**). **Figure 2b** shows that the difference in inclusion pressure $P_{inc} - P_{inc}^{464}$ scales linearly with the differential strain. For large differential strains there is a large difference in inclusion pressure: in the extreme case of some quartz inclusions from piston-cylinder press experiments, the difference in inclusion pressure might exceed

0.6 GPa, for very strained inclusions (Δε < -0.08; alm 1 in **Figure 1** and **2b**; Bonazzi et al., 2019). For this particular inclusion (alm1-grt01-I4), the calculated entrapment pressure (P_{trap}) at 775 °C using the P_{inc}^{464} is 1.67±0.08 GPa, while using the P_{inc} is 2.82±0.28. The P_{trap} was calculated with the software EntraPT (Mazzucchelli et al., 2020) using the EoS for quartz (Angel et al., 2017a) and almandine (Milani et al., 2015). These extreme differential strains are seldom found in natural samples. Nevertheless, natural inclusions from Syros (Cisneros et al., 2020) and Papua New Guinea (Gonzalez et al., 2019) have differential strains ranging from ~-0.03 and 0.02, which correspond to a difference in inclusion pressures from -0.2 to 0.2 GPa (blue and green circles in **Figure 2b**) and a difference in P_{trap} at 550 °C up to 0.7 GPa. As such, the difference in entrapment pressures calculated from P_{inc} and P_{inc}^{464} are geologically significant if the inclusion is under differential strain. However, the entrapment pressure calculated from the P_{inc} is reliable (within uncertainties), even for extreme differential strains.

Implications

Raman elastic geobarometry is a viable tool to measure the strain and stress state of quartz (and zircon) inclusions in garnet and reveals that such inclusions are often under non hydrostatic stress conditions. This observation can provide a reliable starting point for future studies on how to measure and estimate non-lithostatic stresses acting at the scale of the single garnet and whether they can be upscaled to the meso- and macro-scale of the rock units of which they are part.

Inclusion pressures calculated from single mode shifts of quartz are similar to those calculated from the Grüneisen tensor for inclusions under small volume strains ($-0.03 < \varepsilon_V < 0.01$) and near-hydrostatic conditions. The difference between the two methods of calculating inclusion pressures increases drastically with increasing differential strain of the inclusion. Given that quartz inclusions are seldom under hydrostatic stress, the hydrostatic approximation is unreliable and should be avoided.

Acknowledgements

This project received funding from the European Research Council under the European Union’s Horizon 2020 research and innovation program grant agreement 714936 (ERC-STG TRUE DEPTHS) to M. Alvaro. Alvaro has been also supported by the Ministero dell’Istruzione dell’Università e della Ricerca (MIUR)Progetti di Ricerca di

Interesse Nazionale (PRIN)Bando PRIN 2017 - Prot. 2017ZE49E7_005. We thank Jay Thomas and an anonymous reviewer for their comments which helped improve this manuscript.

Figures

Figure 1 – Graph of $\varepsilon_1+\varepsilon_2$ vs. ε_3 displaying the strains of quartz inclusions from piston-cylinder press experiments (Bonazzi et al., 2019) and natural samples from Syros in Greece (Cisneros et al., 2020) and from Papua New Guinea (Gonzalez et al., 2019). The lines in black are the lines of mean normal stress (P_{inc}) of quartz calculated from the room-P stiffness tensor, while the lines in red were calculated using the hydrostatic calibration (P_{inc}^{464}) by Morana et al., 2020. The yellow dashed lines is the hydrostatic stress of quartz (Reuss bound) calculated with the quartz EoS (Angel et al., 2017a). The green dashed line is the isotropic strain (Voigt bound). Further explanation of these types of strain plot is provided in the supplementary materials.

Figure 2 – graph of P_{inc} - P_{inc}^{464} in GPa vs. volume strain (a) and differential strains (b).

References

Angel, R.J. (2000) Equations of state. Reviews in mineralogy and geochemistry, 41(1), 35-59.

Angel, R.J., Alvaro, M., Miletich, R., and Nestola, F. (2017a) A simple and generalised P–T–V EoS for continuous phase transitions, implemented in EosFit and applied to quartz. Contributions to Mineralogy and Petrology, 172(5), 29.

Angel, R.J., Mazzucchelli, M.L., Alvaro, M., and Nestola, F. (2017b) EosFit-Pinc: A simple GUI for host-inclusion elastic thermobarometry. American Mineralogist, 102(9), 1957-1960.

Angel, R.J., Mazzucchelli, M.L., Alvaro, M., Nimis, P., and Nestola, F. (2014) Geobarometry from host-inclusion systems: the role of elastic relaxation. American Mineralogist, 99(10), 2146-2149.

Angel, R.J., Murri, M., Mihailova, B., and Alvaro, M. (2019) Stress, strain and Raman shifts. Zeitschrift für Kristallographie-Crystalline Materials, 234(2), 129-140.

Bonazzi, M., Tumiati, S., Thomas, J.B., Angel, R.J., and Alvaro, M. (2019) Assessment of the reliability of elastic geobarometry with quartz inclusions. Lithos, 350, 105201.

Cisneros, M., Barnes, J.D., Behr, W.M., Kotowski, A.J., Stockli, D.F., and Soukis, K. (2020) Insights from elastic thermobarometry into exhumation of high-pressure metamorphic rocks from Syros, Greece. Solid Earth Discussions, 1-27.

Dunkel, K.G., Zhong, X., Arnestad, P.F., Valen, L.V., and Jamtveit, B. (2020) High transient stress in the lower crust: Evidence from dry pseudotachylytes in granulites, Lofoten Archipelago, Northern Norway. Geology, 49.

Enami, M., Nishiyama, T., and Mouri, T. (2007) Laser Raman microspectrometry of metamorphic quartz: A simple method for comparison of metamorphic pressures. American Mineralogist, 92(8-9), 1303-1315.

Gonzalez, J.P., Thomas, J.B., Baldwin, S.L., and Alvaro, M. (2019) Quartz-in-garnet and Ti-in-quartz thermobarometry: Methodology and first application to a quartzofeldspathic gneiss from eastern Papua New Guinea. Journal of Metamorphic Geology, 37(9), 1193-1208.

Kohn, M.J. (2014) "Thermoba-Raman-try": Calibration of spectroscopic barometers and thermometers for mineral inclusions. Earth and Planetary Science Letters, 388, 187-196.

Mazzucchelli, M.L., Angel, R.J., and Alvaro, M. (2020) EntraPT: an online platform for elastic geothermobarometry. American Mineralogist.

Milani, S., Nestola, F., Alvaro, M., Pasqual, D., Mazzucchelli, M., Domeneghetti, M., and Geiger, C. (2015) Diamond–garnet geobarometry: The role of garnet compressibility and expansivity. Lithos, 227, 140-147.

Morana, M., Mihailova, B., Angel, R.J., and Alvaro, M. (2020) Quartz metastability at high pressure: what new can we learn from polarized Raman spectroscopy? Physics and Chemistry of Minerals, 47(8), 1-9.

Murri, M., Mazzucchelli, M.L., Campomenosi, N., Korsakov, A.V., Prencipe, M., Mihailova, B.D., Scambelluri, M., Angel, R.J., and Alvaro, M. (2018) Raman elastic geobarometry for anisotropic mineral inclusions. American Mineralogist, 103(11), 1869-1872.

Rosenfeld, J.L., and Chase, A.B. (1961) Pressure and temperature of crystallization from elastic effects around solid inclusions in minerals? American Journal of Science, 259(7), 519-541.

Schmidt, C., and Ziemann, M.A. (2000) In-situ Raman spectroscopy of quartz: A pressure sensor for hydrothermal diamond-anvil cell experiments at elevated temperatures. American Mineralogist, 85(11-12), 1725-1734.

Thomas, J.B., and Spear, F.S. (2018) Experimental study of quartz inclusions in garnet at pressures up to 3.0 GPa: evaluating validity of the quartz-in-garnet inclusion elastic thermobarometer. Contributions to Mineralogy and Petrology, 173, 1-14.

Wang, J., Mao, Z., Jiang, F., and Duffy, T.S. (2015) Elasticity of single-crystal quartz to 10 GPa. Physics and Chemistry of Minerals, 42(3), 203-212.

Wolfe, O.M., and Spear, F.S. (2020) Regional Quartz Inclusion Barometry and Comparison with Conventional Thermobarometry and Intersecting Isopleths from the Connecticut Valley Trough, Vermont and Massachusetts, USA. Journal of Petrology.

Zhong, X., Andersen, N.H., Dabrowski, M., and Jamtveit, B. (2019) Zircon and quartz inclusions in garnet used for complementary Raman thermobarometry: application to the Holsnøy eclogite, Bergen Arcs, Western Norway. Contributions to Mineralogy and Petrology, 174(6), 50.

Ziman, J.M. (1960) Electrons and phonons: the theory of transport phenomena in solids. Oxford university press.

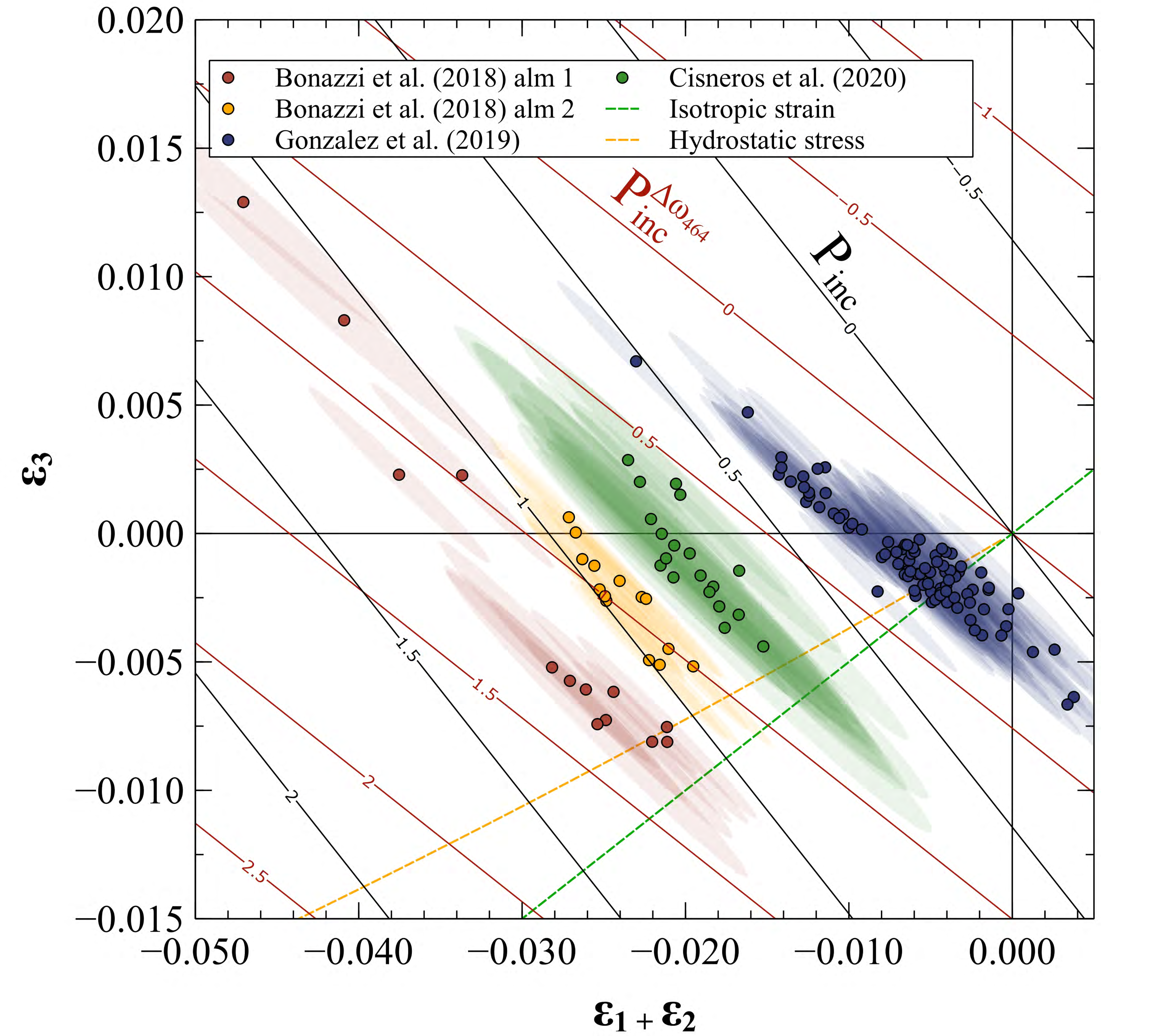

Bonazzi et al. (2018) alm 1
Bonazzi et al. (2018) alm 2
Gonzalez et al. (2019)
Cisneros et al. (2020)
Isotropic strain
Hydrostatic stress
$P_{inc}^{\Delta\omega_{464}}$
P_{inc}
ε_3
$\varepsilon_1 + \varepsilon_2$
0.020
0.015
0.010
0.005
0.000
−0.005
−0.010
−0.015
−0.050
−0.040
−0.030
−0.020
−0.010
0.000
−1
−0.5
0
0.5
1
1.5
2
2.5

a.
Hydrostatic stress
Isotropic strain
$P_{inc} - P_{inc}^{\omega_{464}}$ (GPa)
0.00
−0.25
−0.50
−0.75
−0.10
−0.08
−0.06
−0.04
−0.02
0.00
Volume strain [$\varepsilon_V = \varepsilon_1 + \varepsilon_2 + \varepsilon_3$]
b.
Bonazzi et al. (2018) alm 1
Bonazzi et al. (2018) alm 2
Gonzalez et al. (2019)
Cisneros et al. (2020)
Hydrostatic strain
$P_{inc} - P_{inc}^{\omega_{464}}$ (GPa)
0.60
0.40
0.20
0.00
−0.20
−0.06
−0.05
−0.04
−0.03
−0.02
−0.01
0.00
0.01
0.02
Differential strain [$\Delta\varepsilon = \varepsilon_1 - \varepsilon_3$]